

Calculations for Steady Propagation of a Generic Ram Accelerator Configuration

Matthew J. Grismer* and Joseph M. Powers†
University of Notre Dame, Notre Dame, Indiana 46556

This study describes a methodology and gives analysis to determine the steady propagation speed of a projectile fired into a gaseous mixture of fuel and oxidizer. So that numerical results can be analytically verified in limiting cases, a simple model and geometry are used: the steady supersonic flow of an inviscid, calorically perfect, ideal, reacting gas with high activation energy over an unconfined symmetric double wedge is considered. Typical predicted flowfields consist of a lead inert oblique shock followed by a thick induction zone, thin reaction zone, rarefaction, and trailing oblique shock. The reaction strengthens the lead shock to the extent that the far-field wave angle is that of a Chapman-Jouguet (*CJ*) oblique detonation. Propagation speeds are found that give rise to shocks of such strength as to induce the reaction zone to be in a region that allows the combustion-induced thrust to balance the wave drag. For a fixed heat release greater than a critical value, two steady propagation speeds are predicted. The solution at the higher Mach number is stable to quasistatic perturbations, whereas the solution at the lower Mach number is unstable. The steady solutions are superdetonative in that the projectile velocities that give rise to force balances are greater than the *CJ* velocity for a detonation wave aligned normal to the direction of projectile motion. This methodology can be applied to analyze devices that have more complex geometries, such as the ram accelerator or oblique detonation wave engine.

Introduction

It is possible to employ oblique shock waves to induce combustion to generate thrust. Recent discussion has been motivated by the ram accelerator, which has been used to propel projectiles to high speeds, and the oblique detonation wave engine (ODWE), which has been proposed to propel the National Aerospace Plane (NASP). For such devices, it is of fundamental importance to have a theory that can predict a steady propagation speed. To this end, a Rankine-Hugoniot analysis that utilized a thermal explosion theory was performed by Powers and Gonthier,¹ and was qualitatively verified in a numerical analysis by Powers et al.² Additionally, the numerical analyses of Brackett and Bogdanoff³ and Yungster and Bruckner,⁴ which model ram accelerators powered by $H_2 - O_2$ combustion, suggest that steady velocities in the range 5000–10,000 m/s may be achievable, although in these studies only a small number of steady propagation speeds were found.

In this article we briefly review some of the relevant literature, describe a general methodology for determining the steady propagation speed of either ram accelerator projectiles or ODWE-powered aerospace planes, pose a simple model problem to illustrate the methodology, give the results of a numerical analysis, and finish with a brief discussion. Much of the substance of this article was first given in Refs. 1 and 2; however, the early results lacked quantitative accuracy due to highly smeared shock fronts and restrictions imposed by thermal explosion theory. This article extends and improves the previous work through the use of a new code based on the Roe method⁵ to achieve a much-improved resolution near discontinuities. Because the model and geometry employed here are particularly simple, it was possible to verify the code

by comparing its predictions to a number of one- and two-dimensional inert and reactive exact solutions. The main new contributions of this article, in combination with Refs. 1 and 2, are 1) a numerically verified theory for the dependency of steady propagation speed on heat release, and 2) a numerically verified theory for the far-field flowfield behavior.

Review

The ram accelerator (see Fig. 1) was first tested by Hertzberg et al.^{6,7} In this application, a high-speed projectile is fired into a tube filled with an unreacted mixture of combustible gases. In one test a 70-g projectile was fired into a 16-m-length, 38-mm-bore tube filled in its first three stages with varying combinations of CH_4 , O_2 , N_2 , and He at a pressure of 31 bar, and in its final stage with $0.9 C_2H_4 + 3O_2 + 5CO_2$ at a pressure of 16 bar. A shock-induced combustion process accelerated the projectile from an initial velocity of near 1200 m/s to a velocity of 2475 m/s (corresponding to a Mach number $M = 8.4$) at the end of the tube, at which location it was still accelerating. Downstream pressures near 600 bar were measured. The diameter of the projectile's main body was 28.9 mm. Its length was 166 mm, and the leading-edge conical half-angle $\theta = 10$ deg. Four stabilizing fins (not shown) of diameter 38 mm were a part of the aft-body. A portion of the oblique shock train is sketched in Fig. 1; the various expansion fans and wave interactions are not included. Figure 1 depicts the first reflected shock triggering significant chemical reac-

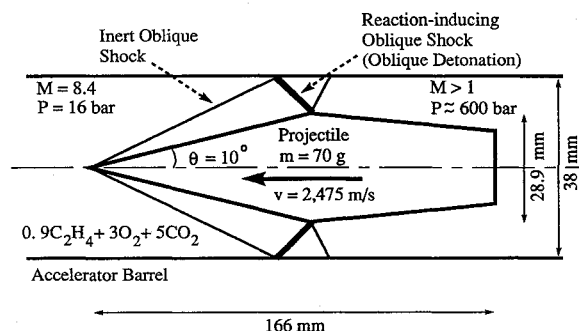


Fig. 1 Schematic of ram accelerator, adopted from Hertzberg et al.⁷

Received Dec. 8, 1993; presented as Paper 94-0550 at the AIAA 32nd Aerospace Sciences Meeting and Exhibit, Reno, NV, Jan. 10–13, 1994; revision received May 10, 1994; accepted for publication May 23, 1994. Copyright © 1994 by the American Institute of Aeronautics and Astronautics, Inc. All rights reserved.

*Graduate Research Assistant, Department of Aerospace and Mechanical Engineering; currently assigned to Wright Laboratory, Wright-Patterson AFB, OH. Student Member AIAA.

†Assistant Professor, Department of Aerospace and Mechanical Engineering. Member AIAA.

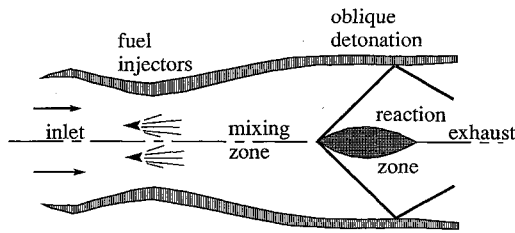


Fig. 2 Envisioned oblique detonation wave engine, adopted from Dunlap et al.¹⁰

tion; the temperature-sensitive reaction would be associated with the lead shock for faster projectile speeds, and with a downstream shock for slower speeds. For even slower speeds, the reaction would either be downstream of the projectile or a normal detonation running ahead of the projectile would be triggered. It was suggested that such a device can be scaled for direct launch to orbit, for hypervelocity impact studies, and for a hypersonic test facility.

Another relevant propulsion device is the proposed ODWE. The idea of the ODWE has existed for decades (e.g., Dunlap et al.¹⁰). The hypothesized operation is as follows (see Fig. 2). Supersonic air enters the inlet. On-board fuel is injected downstream that mixes with the air without significant reaction. The mixture then encounters a downstream wedge. The oblique shock associated with the wedge compresses and ignites the mixture, generating a propulsive force. Relative to conventional air-breathing engines, Dunlap et al. cite the ODWE's advantages as 1) simpler inlet diffuser design since the inherently supersonic oblique detonation does not require deceleration to a subsonic state, 2) reduced total pressure losses, 3) shorter combustion chamber length, 4) no ignition device other than the wedge, and 5) faster flight velocities. Cited concerns are 1) the lack of static thrust, 2) uncertainty as to whether mixing lengths are practical, and 3) uncertainty of the process's stability.

Methodology and Model Problem

Most recent theoretical studies related to ram accelerators and ODWEs⁸⁻²⁴ have not given detailed analyses focused on determining a steady propagation speed, i.e., the terminal velocity. Typically, the related problem of flow with a fixed incoming Mach number over a fixed geometry is examined. Emphasis is placed on characterizing the resulting flowfield, and only a small number of incoming Mach numbers are studied. This approach does yield the thrust force as a function of flight speed, but in general does not give the upper velocity bound for the device.

Here we present a general approach to predict the steady speed. One first selects a mathematical model for the fluid and a representative geometry. The model equations are studied in the reference frame in which the projectile is stationary; thus, the incoming flow velocity, which is the steady propagation speed, is thought of as an adjustable parameter at this stage. For a given incoming velocity, solution of the model equations leads to a stress distribution on the projectile surface that may or may not result in a net force on the projectile. Should the particular incoming velocity lead to no net force, that velocity is a candidate for a steady propagation speed. The static stability of the candidate solution is easily determined. Should a perturbation in the incoming velocity lead to a net force that tends to restore the projectile to a speed at which there is no net force, the solution is stable in a static sense (we call such solutions stable); otherwise, the solution is unstable. A further step, not considered here, is to account for the inertia of the projectile and surrounding fluid so as to determine the dynamic stability.

This methodology is illustrated through the use of a model problem that is related to the ram accelerator and ODWE. So that our numerical results can be verified by analytic solutions in certain limits, we consider an idealized model and

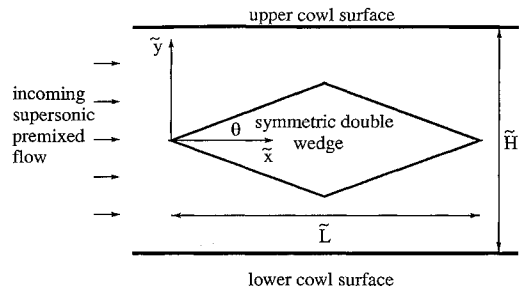


Fig. 3 Schematic of generic configuration.

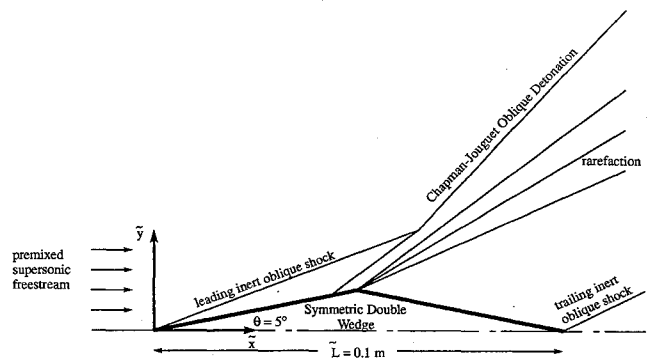


Fig. 4 Detailed schematic for $\tilde{H} \rightarrow \infty$.

geometry that retain essential features of real systems. The geometry, shown in Fig. 3, is a symmetric double wedge with half angle θ and length \tilde{L} . Two cowl surfaces are placed symmetrically about the wedge and are separated by height \tilde{H} . The depth of the double wedge and cowl is taken to be infinite, and the flow is assumed to have no variation in this direction. The Cartesian coordinate system, with its origin at the leading edge and with the \tilde{x} axis aligned with the incoming flow, is also indicated. It is appropriate to think of a ram accelerator as the axisymmetric analog in which the projectile moves while the cowl is stationary; likewise, an aerospace plane powered by an ODWE can be thought of as the axisymmetric analog in which the cowl moves with the wedge. In both scenarios one must assume that the incoming fuel and oxidizer are completely mixed; in actuality this is more appropriate for the ram accelerator than the ODWE.

Analysis of the geometry of Fig. 3 leads in general to a complicated interaction of shocks, rarefactions, and combustion processes as the flow passes between the projectile and cowl surface. To further simplify, we consider only the limit $\tilde{H} \rightarrow \infty$, Fig. 4. Consequently, our geometry bears only a rudimentary resemblance to actual devices, but has the advantage of being amenable to simple analysis.

Again for tractability, the flow model employed also has only a rudimentary resemblance to commonly used models for real fluids. We consider an inviscid calorically perfect ideal reacting gas with one-step irreversible Arrhenius kinetics; the reactants and products are taken to have the same molecular weights and material properties. Figure 4 indicates typical flow features. The ambient, premixed freestream fluid encounters an attached oblique shock at the leading edge of the projectile. No appreciable reaction occurs within the shock or near the front of the projectile. Near the apex of the wedge appreciable reaction begins, and at the apex the flow is turned through a rarefaction until it attains a velocity parallel to the lee wedge surface. The reaction then proceeds to completion on the leeward side of the projectile. The flow passes through a final oblique shock at the tail of the projectile, resulting in a velocity only in the \tilde{x} direction. The net force on the projectile is determined by integrating the pressure over the entire surface area. The lead oblique shock wave is strengthened by the reaction such that in the far field the shock angle

reaches the Chapman-Jouguet (CJ) wave angle, as will be demonstrated in this article.

Model Equations

The dimensionless model equations are given below:

$$\frac{d\rho}{dt} + \rho \frac{\partial v_i}{\partial x_i} = 0 \quad (1)$$

$$\frac{dv_i}{dt} + \frac{1}{\rho} \frac{\partial P}{\partial x_i} = 0 \quad (2)$$

$$\frac{de}{dt} - \frac{P}{\rho^2} \frac{d\rho}{dt} = 0 \quad (3)$$

$$\frac{d\lambda}{dt} = \kappa(1 - \lambda) \exp\left(-\frac{\Theta}{T}\right) \quad (4)$$

$$e = \frac{1}{\gamma - 1} \frac{P}{\rho} - \lambda q \quad (5)$$

$$P = \rho T \quad (6)$$

The dependent variables in Eqs. (1–6) are the density ρ , the Cartesian velocity component v_i , the pressure P , the internal energy e , the temperature T , and the reaction progress variable λ . The independent variables are time t and the Cartesian position coordinate x_i . The dimensionless parameters are the ratio of specific heats γ , the kinetic rate constant κ , the heat of reaction q , and the activation energy Θ . Here the material derivative $(d/dt) = (\partial/\partial t) + v_i(\partial/\partial x_i)$.

Equations (1–3) express conservation principles for mass, momenta, and energy, respectively. Equation (4) is a species evolution equation that incorporates an Arrhenius depletion model. Equations (5) and (6) are caloric and thermal equations of state. A single, first-order, irreversible, exothermic reaction is employed, $A \rightarrow B$. The reaction progress variable λ ranges from zero before reaction to unity at complete reaction. Species mass fractions, Y_A , Y_B , are related to the reaction progress variable by the formulas, $Y_A = 1 - \lambda$, $Y_B = \lambda$.

In Eqs. (1–6) pressure, density, and temperature are scaled so their preshock values are unity; velocities are scaled by a number closely related to the preshock acoustic speed. The length of the projectile \bar{L} is chosen as the reference length scale. The reference time is of the same order of magnitude as the time for a fluid particle to traverse the length of the projectile. In terms of dimensional (indicated by the notation “”) variables, parameters, and preshock ambient conditions (indicated by the subscript “0”), the dimensionless variables are defined by

$$\begin{aligned} \rho &= \frac{\bar{\rho}}{\bar{\rho}_0}, & P &= \frac{\bar{P}}{\bar{P}_0}, & e &= \frac{\bar{e}}{\bar{P}_0/\bar{\rho}_0} \\ T &= \frac{\bar{R}}{\bar{P}_0/\bar{\rho}_0} \bar{T}, & u &= \frac{\bar{u}}{\sqrt{\bar{P}_0/\bar{\rho}_0}}, & v &= \frac{\bar{v}}{\sqrt{\bar{P}_0/\bar{\rho}_0}} \\ x &= \frac{\bar{x}}{\bar{L}}, & y &= \frac{\bar{y}}{\bar{L}}, & t &= \frac{\sqrt{\bar{P}_0/\bar{\rho}_0}}{\bar{L}} \bar{t} \end{aligned} \quad (7)$$

The dimensionless parameters are defined by the following relations:

$$\begin{aligned} q &= \frac{\bar{q}}{\bar{P}_0/\bar{\rho}_0}, & \Theta &= \frac{\bar{E}}{\bar{P}_0/\bar{\rho}_0}, & \gamma &= 1 + \frac{\bar{R}}{\bar{c}_v} \\ \kappa &= \frac{\bar{L}}{\sqrt{\bar{P}_0/\bar{\rho}_0}} \bar{\kappa}, & M_0 &= \frac{\bar{u}_0}{\sqrt{\gamma \bar{P}_0/\bar{\rho}_0}} \end{aligned} \quad (8)$$

Here, M_0 is the freestream Mach number that is required in the initial preshock conditions. The dimensional parameters are \bar{q} the heat of reaction, \bar{E} the activation energy, \bar{R} the gas constant for the particular fluid, \bar{c}_v the specific heat at constant volume, and \bar{k} the kinetic rate constant. With this scaling, initial preshock conditions are specified as $\rho = 1$, $u = \sqrt{\gamma M_0}$, $v = 0$, $P = 1$, $T = 1$, $e = 1/(\gamma - 1)$, and $\lambda = 0$.

Numerical Analysis

A numerical analysis of Eqs. (1–6) was performed using a new code²⁵ based on the Roe method. In brief, the code uses an explicit Roe scheme⁵ and fractional stepping to integrate the equations in a generalized, curvilinear coordinate system. The integration has second-order spatial accuracy in smooth regions of the flowfield and first-order temporal accuracy. In the implementation of the Roe scheme, all eigenvalues and eigenvectors of the generalized flux Jacobian matrices were obtained analytically, resulting in an efficient and robust code. The second-order spatial accuracy was obtained using a version of the higher-order total-variation-diminishing (TVD) schemes for Roe averaging suggested by Chakravarthy and Osher.²⁶

The code works in a finite volume sense, requiring flux boundary conditions on all sides of the domain. At the inflow, all fluxes were specified based upon the chosen inflow quantities. At the projectile surface, slip wall boundary fluxes were specified by setting the transverse component of the velocity (in the curvilinear space) to zero. The only nonzero components of the transverse flux then involved the pressure at the projectile surface. This was estimated by using one-dimensional Riemann invariants and the nearest cell centered quantities, as suggested by Dadone and Grossman.²⁷ Lastly, the nonreflective boundary conditions suggested by Thompson²⁸ were specified at the outflow. This method utilizes the characteristic formulation of the equations to remove reflections from the outflow boundary. Basically, outflowing characteristics are calculated with upwind differencing, while any inflowing characteristics are set to zero. The boundary at the top of the computational domain was treated as a wall, but this had no effect on the solutions presented here since in all cases the far-field oblique detonation exited through the rear boundary without touching the top of the domain.

One-dimensional inert and reactive test cases were used to verify the method. First, the classical Riemann shock-tube problem was considered (see, e.g., Hirsch,²⁹ pp. 204–211) for a calorically perfect inert ideal gas [$\gamma = \frac{5}{3}$, $\bar{R} = 287$ J/(kgK)]. Figure 5 gives instantaneous pressure, density, and particle velocity profiles at $\bar{t} = 39$ ms. Dimensional initial conditions were specified as $\bar{P} = 10^5$ Pa, $\bar{\rho} = 1$ kg/m³, $\bar{u} = 0$ m/s for $0 \text{ m} < \bar{x} < 5$ m, and $\bar{P} = 10^3$ Pa, $\bar{\rho} = 10^{-2}$ kg/m³, $\bar{u} = 0$ m/s for $5 \text{ m} < \bar{x} \leq 10$ m. In Fig. 5, a slightly different scaling has been used, more appropriate to this problem; i.e., density, velocity, and pressure have been scaled by their peak

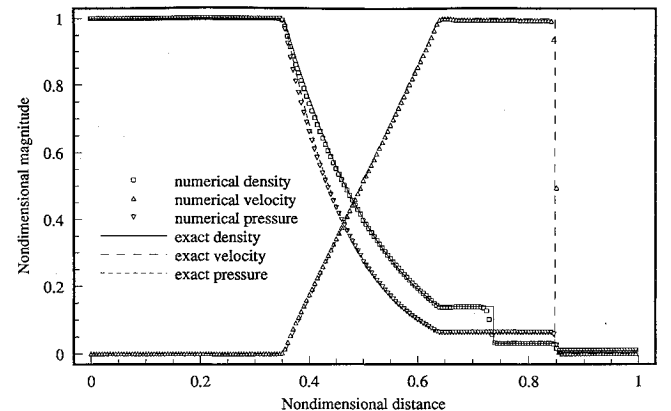


Fig. 5 Exact and numerical inert Riemann shock-tube problem solutions.

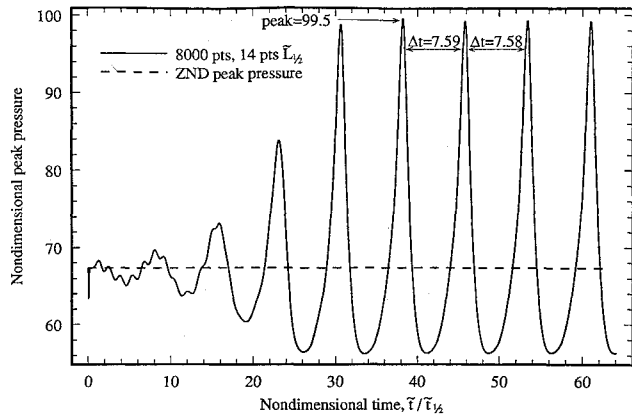


Fig. 6 Unsteady ZND detonation ($f = 1.6$, $\Theta = 50$, $q = 50$, $\gamma = 1.2$).

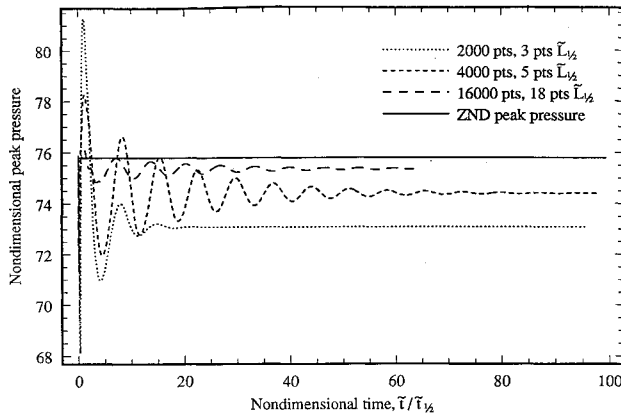


Fig. 7 Steady ZND detonation ($f = 1.8$, $\Theta = 50$, $q = 50$, $\gamma = 1.2$).

values, and distance has been scaled by the tube length, 10 m. The domain was broken into 200 uniform cells; no mesh adaptation was used. The numerical method does an excellent job of matching the exact solution. The weakest agreement is near the contact discontinuity, which is apparent in the first "step" of the density curve. Shock discontinuities, present in all the variables' profiles, are captured well in only a few points.

A more stringent test of the method was considered next. It is well-known that for certain values of q , Θ , and overdrive f , one-dimensional detonation solutions of Eqs. (1–6), known as Zeldovich-von Neumann-Doering (ZND) detonations, are unstable. Here, overdrive is defined as $f = (D/D_{CJ})^2$, where D is the speed of a piston-supported traveling detonation, and D_{CJ} is the speed of an unsupported, freely traveling detonation. Fickett and Davis³⁰ review most of the early stability studies; Lee and Stewart³¹ give a recent linear analysis. Among others, Fickett and Wood,³² and more recently Bourlioux et al.,³³ have calculated the nonlinear behavior of these unstable detonations.

Since the linear stability limits are known,³¹ a good test of a method is to see if it correctly predicts solutions near stability boundaries. We present results for two cases, the first on the unstable side of the boundary (Fig. 6), the other on the stable side (Fig. 7). In both cases, the initial conditions were the exact, steady ZND detonation found from integration of the ordinary differential equations that arise in the steady wave frame. The legends of each figure indicate the total number of points used in the computational domain, as well as the number of points contained in the half-reaction zone length $\bar{L}_{1/2}$ of the initial ZND solution. The half-reaction zone length is defined as the distance in a steady solution between the detonation front and the point at which the reaction is half complete $\lambda = \frac{1}{2}$. Also, for ease of comparison, the nondimensional time shown is that of Ref. 32, in which the scaling

parameter is the time $\bar{t}_{1/2}$ for a fluid particle to cross the half-reaction zone length.

Figure 6 shows the peak pressure at the front of the detonation vs time for an unstable detonation ($f = 1.6$, $\Theta = 50$, $q = 50$, $\gamma = 1.2$). The numerical method predicts a peak pressure that oscillates about that predicted by the steady ZND solution. The amplitude and period of the oscillation agree well with previous solutions.³³ Figure 7 shows the same plot for a stable detonation ($f = 1.8$, $\Theta = 50$, $q = 50$, $\gamma = 1.2$). The solution exhibits initial oscillations; these dampen, and the peak pressure correctly approaches a long-time value close to the independently-predicted ZND peak pressure. Using more points in the computational domain resulted in the numerical solution more closely approaching the ZND peak pressure. A number of cases even closer to the stability boundaries were examined, and in each the method correctly predicted the steady or unsteady behavior.

Results

For the unconfined double wedge, steady propagation speeds were sought that gave rise to a force balance as the heat release parameter q was varied, $11.908 \leq q \leq 13.456$. Other parameters were held constant at $\gamma = 7/5$, $\theta = 5$ deg, $\Theta = 12.32$, and $\kappa = 9179$. For presentation of results dimensional parameters were chosen as $\bar{P}_0 = 1.01325 \times 10^5$ Pa, $\bar{\rho}_0 = 1.225$ kg/m³, $\bar{k} = 2.64 \times 10^7$ s⁻¹, $\bar{E} = 1.019 \times 10^6$ J/kg, $\bar{L} = 0.1$ m, $\bar{R} = 287$ J/(kgK), $\bar{c}_v = 717.5$ J/(kgK), 0.985×10^6 J/kg $\leq \bar{q} \leq 1.113 \times 10^6$ J/kg. These values were chosen after a search for parametric values that would give rise to a force balance. Their specific value is thus primarily motivated by a desire to illustrate our methodology rather than a goal of precise prediction of a real physical system. A common 199×99 fixed computational grid was used in all cases. Doubling the grid resolution in both directions yielded results with only slight quantitative changes. Convergence to steady state was typically achieved in about 5000 time iterations. At this point the unsteady residuals, $\bar{\Psi}_k^n \equiv \sum_{i=1}^N \sum_{j=1}^M |\Psi_{ijk}^n - \Psi_{ijk}^{n-1}|/NM$, were all near 10^{-6} . Here, $\bar{\Psi}_k^n$ and Ψ_k^n are, respectively, the average and local residual at time $t_n = n\Delta t$ in either ρ , u , v , P , or $e + (u^2 + v^2)/2$. Also, i and j are spatial indices, N and M are the total number of points in the x and y directions, respectively, and n is a temporal index. A typical simulation required about three h of computing time on an IBM RS/6000 POWERstation 350 having 64 Mb RAM and rated at 18.6 MFlops.

The CJ Mach number ($M_{0,CJ}$) for a detonation with a lead shock normal to the flow direction is determined solely by q and γ ³⁰; for the parameters listed $4.275 \leq M_{0,CJ} \leq 4.517$. For cases attempted in which $M_0 \leq M_{0,CJ}$, a normal detonation would form and propagate forward in the domain until it hit the inflow boundary. This corresponds to the detonation attempting to reach its natural, unsupported propagation speed. All cases considered here in which force balances were found had an incoming Mach number well above $M_{0,CJ}$ ($5.5 \leq M_0 \leq 8.5$); consequently, the steady propagation speeds we find are in what is commonly known as the superdetonative regime.

The projectile achieves a steady velocity when the force due to pressure wave drag, which tends to retard the motion, is balanced by the thrust force induced by combustion, which tends to accelerate the projectile. The dimensionless net force per unit depth F_{net} is given by the pressure force integrated over the circumference of the diamond-shaped wedge: $F_{net} = \oint P n_i ds$, where n_i is the unit normal to the surface and ds is an element of arc length of the diamond-shaped wedge of Fig. 3. This integral is evaluated numerically. Due to symmetry, the only nonzero component of F_{net} is in the x direction. This force is defined to be positive if it points in the negative x direction. Figure 8 shows F_{net} plotted vs M_0 for the three indicated values of \bar{q} .

For low heat release F_{net} is negative; the thrust force induced by combustion is not sufficient to overcome the wave drag. At a critical value of heat release, $\bar{q} = 0.992$ MJ/kg

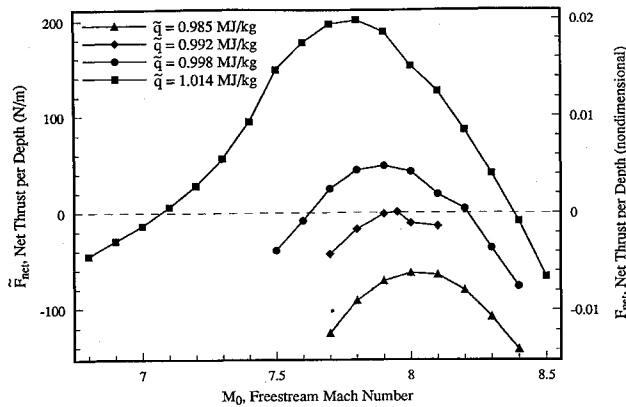


Fig. 8 Net thrust force vs Mach number for varying heat release.

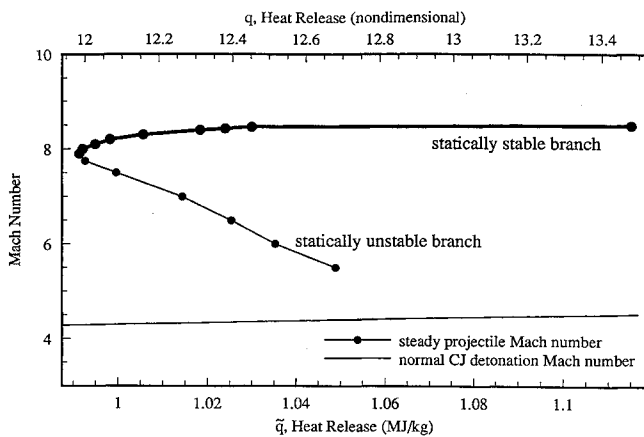


Fig. 9 Bifurcation diagram for steady-state speed vs heat of reaction.

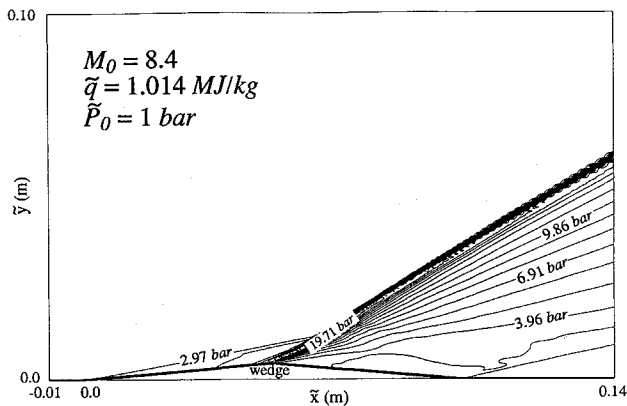


Fig. 10 Pressure contours for statically stable steady configuration.

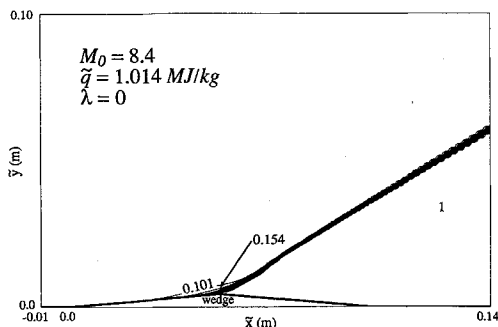


Fig. 11 Product mass fraction contours for statically stable configuration.

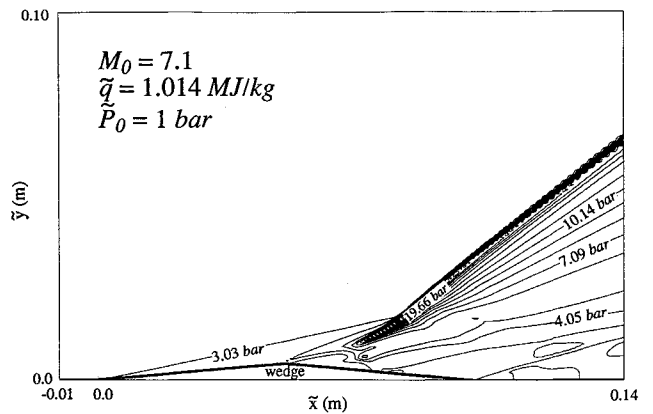


Fig. 12 Pressure contours for statically unstable steady configuration.

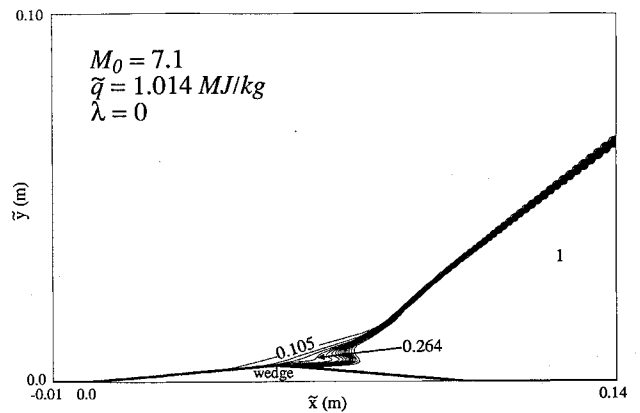


Fig. 13 Product mass fraction contours for statically unstable steady configuration.

($q = 11.993$), there is a balance of combustion-induced thrust and drag such that $F_{\text{net}} = 0$. This occurs at $M_0 = 7.95$. For larger values of heat release, there are two distinct Mach numbers for which $F_{\text{net}} = 0$. A perturbation in the Mach number for the steady solution at the lower Mach number results in a net force that tends to accelerate the projectile away from the equilibrium Mach number. Consequently, this is a statically unstable equilibrium. In the same manner, the equilibrium solution at the higher Mach number is statically stable to such perturbations.

These results are summarized in the bifurcation diagram shown in Fig. 9, where equilibrium Mach numbers M_0 vs heat release \bar{q} (and q) are plotted. The lower branch is unstable, whereas the upper branch is stable. On the stable branch near the bifurcation point, an increase in \bar{q} causes the flight speed to increase. The solutions shown here correspond to stable flight speeds in the range of $2700 \text{ m/s} \lesssim \bar{u}_0 \lesssim 2900 \text{ m/s}$, $7.9 \lesssim M_0 \lesssim 8.5$. To illustrate the superdetonative nature of the results, Fig. 9 also plots the CJ Mach number for a normal detonation vs heat release.

For a particular value of heat release, $\bar{q} = 1.014 \text{ MJ/kg}$, detailed plots of pressure contours and product mass fraction λ contours are given for the stable case $M_0 = 8.4$, and the unstable case $M_0 = 7.1$, in Figs. 10, 11, 12, and 13, respectively. In the stable configuration, the reaction induces the lead oblique shock to undergo a sudden increase in angle of inclination from near 11 to 31 deg. A similar rise from 12 to 38 deg occurs for the unstable case. The reaction occurs sooner for the stable case that is at the higher Mach number. This is readily apparent in the product mass fraction contours. Along the wedge surface chemical reaction reaches completion near the apex for the stable case, while in the unstable case the reaction completes further downstream. This may be explained in the following way: for low M_0 , chemical reaction

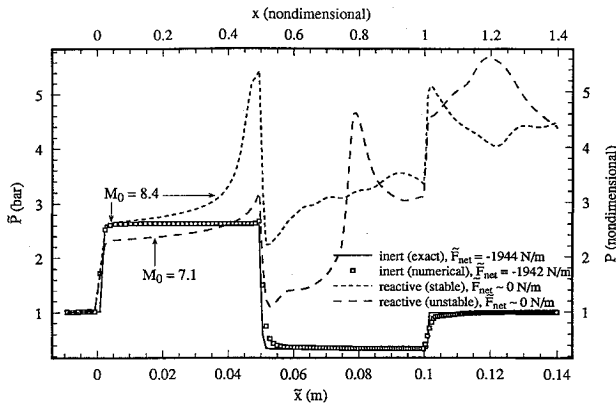


Fig. 14 Pressure traces on wedge surface.

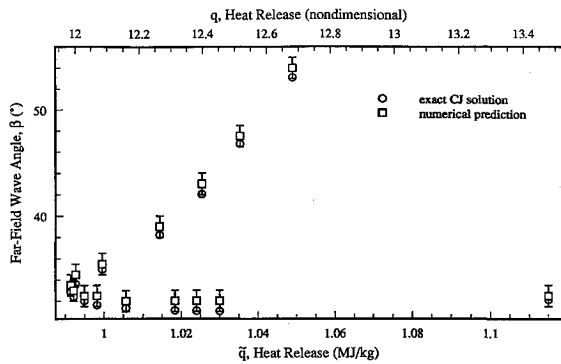


Fig. 15 Numerically predicted far-field wave angle and analytically predicted CJ wave angle vs heat release q ; M_0 varied to maintain force balance, $5.5 \leq M_0 \leq 8.5$.

occurs off the leeward wedge surface far downstream, resulting in a $F_{net} < 0$. As the Mach number is increased, the reaction moves forward onto the wedge, eventually reaching a point at which the wave drag of the projectile is balanced by the thrust due to chemical reaction. Increasing M_0 past this equilibrium point moves the reaction closer to the wedge apex on the leeward side, resulting in positive F_{net} . Increasing M_0 still further pushes the reaction over the apex and onto the front of the wedge. The pressure increase due to chemical reaction on the front of the wedge is then balanced by the resulting higher pressure on the leeward side of the wedge.

Figure 14 shows plots of the pressures along the lines of symmetry and projectile surface for the stable and unstable cases of interest. Here there are about 90 grid points distributed on the wedge surface. As a verification of the code's ability to predict two-dimensional flows, plots of the exact and numerical pressure traces for an inert flow over the projectile are also given. The numerical pressure closely follows the exact solution, showing the biggest discrepancies at the shock and rarefaction discontinuities. The discontinuities are still captured well, however, and there is no evidence of any Gibbs phenomena. Drag calculations for the exact and numerical solutions show that they are in excellent agreement.

For the stable case, Fig. 14 indicates significant reaction on the front face of the wedge. The pressure rises slowly following the lead shock, and then rapidly prior to the rarefaction at the wedge apex. Following the apex the pressure remains above that of the inert case, and then jumps again through the trailing shock at the end of the projectile. The unstable case has a different character. Again, the pressure rises slowly following the lead shock, but the peak prior to the rarefaction is lower. The pressure drops through the rarefaction, but again is above that of the inert case. The pressure peaks on the back of the wedge where the reaction reaches completion, and then jumps through the trailing shock.

Lastly, in the far-field limit the numerical results strongly suggest that the lead oblique shock has been strengthened by

the reaction so as to evolve into a CJ oblique detonation. This result gives numerical confirmation to ideas put forth by Chernyi.³⁴ As discussed in detail in many sources (see, e.g., Refs. 14, 16, and 17), the CJ oblique detonation is the unique oblique detonation that has at the end of the reaction zone a velocity component normal to the shock front that is locally sonic. For each of the cases in which a force balance existed as plotted in Fig. 9, the far-field shock wave angle β was graphically measured and compared to the analytically known CJ wave angle β_{CJ} . These results are plotted in Fig. 15. It is seen that the analytic prediction is in agreement with the numerical prediction within the limits of accuracy (shown by the error bars) with which the numerically predicted angle can be determined. It was also noted that in cases in which the incoming Mach number did not give rise to a force balance, the far-field behavior was that of a CJ oblique detonation.

Discussion

For the model considered, this article has shown that a force balance and consequent terminal velocity is achieved when the reaction zone length scale is of the same order of magnitude as the projectile's geometric length scale. The trends of 1) the variation of net thrust with Mach number for fixed heat release and 2) the variation of steady propagation speed with variable heat release are consistent with those of Refs. 1 and 2 that used methods that were not as quantitatively accurate as that of the present article.

The results also demonstrate that the CJ condition has only limited relevance in this problem. As the normal CJ velocity is independent of reaction kinetics and the steady flight speed is dependent on kinetics, the two are clearly independent. The only significance of the normal CJ Mach number is as an overly conservative lower bound for flight speeds. Furthermore, as the CJ oblique detonation angle is predicted in the far field for cases with and without force balances, it plays no role in the determination of the steady flight speed.

The results presented here suggest, but do not prove, the flow is stable, since the code is time accurate and the numerical method has demonstrated capability of capturing one-dimensional instabilities. Our resolution yielded between three and four cells within the reaction zone; one-dimensional simulations of piston-driven detonations indicate this may be sufficient, but that more points in the reaction zone would be desirable. Interestingly, the far-field CJ oblique detonation appears stable, although its one-dimensional piston-driven equivalent is known to be unstable. The oblique detonation stability question may be better addressed by a linearized analysis in combination with higher resolution numerical simulations.

Acknowledgments

This study received partial support from the Indiana Space Grant Consortium sponsored by NASA Headquarters. The authors acknowledge John R. Roof IV, who with the support of the NASA-sponsored Research Experience for Undergraduates program, assisted with many numerical calculations. Additionally, a conversation with David T. Pratt of the University of Washington, Seattle, Washington, was very helpful in interpreting our results.

References

- ¹Powers, J. M., and Gonthier, K. A., "Methodology and Analysis for Determination of Propagation Speed of High-Speed Propulsion Devices," *Proceedings of the Central States Section Spring 1992 Technical Meeting of the Combustion Institute*, Ohio State Univ., Columbus, OH, 1992, pp. 1-6.
- ²Powers, J. M., Fulton, D. R., Gonthier, K. A., and Grismer, M. J., "Analysis for Steady Propagation of a Generic Ram Accelerator/Oblique Detonation Wave Engine," AIAA Paper 93-0243, Jan. 1993.
- ³Brackett, D. C., and Bogdanoff, D. W., "Computational Inves-

tigation of Oblique Detonation Ramjet-in-Tube Concepts," *Journal of Propulsion and Power*, Vol. 5, No. 3, 1989, pp. 276–281.

⁴Yungster, S., and Bruckner, A. P., "Computational Studies of a Superdetonative Ram Accelerator Mode," *Journal of Propulsion and Power*, Vol. 8, No. 2, 1992, pp. 457–463.

⁵Roe, P. L., "Approximate Riemann Solvers, Parameter Vectors, and Difference Schemes," *Journal of Computational Physics*, Vol. 43, No. 2, 1981, pp. 357–372.

⁶Hertzberg, A., Bruckner, A. P., and Bogdanoff, D. W., "Ram Accelerator: A New Chemical Method for Accelerating Projectiles to Ultrahigh Velocities," *AIAA Journal*, Vol. 26, No. 2, 1988, pp. 195–203.

⁷Hertzberg, A., Bruckner, A. P., and Knowlan, C., "Experimental Investigation of Ram Accelerator Propulsion Modes," *Shock Waves*, Vol. 1, 1991, pp. 17–25.

⁸Yungster, S., Eberhardt, S., and Bruckner, A. P., "Numerical Simulation of Hypervelocity Projectiles in Detonable Gases," *AIAA Journal*, Vol. 29, No. 2, 1991, pp. 187–199.

⁹Yungster, S., "Numerical Study of Shock-Wave/Boundary-Layer Interactions in Premixed Combustible Gases," *AIAA Journal*, Vol. 30, No. 10, 1992, pp. 2379–2387.

¹⁰Dunlap, R., Brehm, R. L., and Nicholls, J. A., "A Preliminary Study of the Application of Steady-State Detonative Combustion to a Reaction Engine," *Jet Propulsion*, Vol. 28, No. 7, 1958, pp. 451–456.

¹¹Cambier, J. L., Adelman, H., and Menees, G. P., "Numerical Simulations of Oblique Detonations in Supersonic Combustion Chambers," *Journal of Propulsion and Power*, Vol. 5, No. 4, 1989, pp. 483–491.

¹²Cambier, J. L., Adelman, H., and Menees, G. P., "Numerical Simulations of an Oblique Detonation Wave Engine," *Journal of Propulsion and Power*, Vol. 6, No. 3, 1990, pp. 315–323.

¹³Bruckner, A. P., Knowlan, C., Hertzberg, A., and Bogdanoff, D. W., "Operational Characteristics of the Thermally Choked Ram Accelerator," *Journal of Propulsion and Power*, Vol. 7, No. 5, 1991, pp. 828–836.

¹⁴Pratt, D. T., Humphrey, J. W., and Glenn, D. E., "Morphology of Standing Oblique Detonation Waves," *Journal of Propulsion and Power*, Vol. 7, No. 5, 1991, pp. 837–845.

¹⁵Bogdanoff, D. W., "Ram Accelerator Direct Space Launch System: New Concepts," *Journal of Propulsion and Power*, Vol. 8, No. 2, 1992, pp. 481–490.

¹⁶Powers, J. M., and Stewart, D. S., "Approximate Solutions for Oblique Detonations in the Hypersonic Limit," *AIAA Journal*, Vol. 30, No. 3, 1992, pp. 726–736.

¹⁷Powers, J. M., and Gonthier, K. A., "Reaction Zone Structure for Strong, Weak Overdriven, and Weak Underdriven Oblique Detonations," *Physics of Fluids A*, Vol. 4, No. 9, 1992, pp. 2082–2089.

¹⁸Grismer, M. J., and Powers, J. M., "Comparisons of Numerical Oblique Detonation Solutions with an Asymptotic Benchmark," *AIAA Journal*, Vol. 30, No. 12, 1992, pp. 2985–2987.

¹⁹Pepper, D. W., and Brueckner, F. P., "Simulation of an Oblique

Detonation Wave Scramaccelerator for Hypervelocity Launchers," *Computers and Computing in Heat Transfer Science and Engineering*, edited by W. Nakayama and K. T. Yang, CRC Press, Boca Raton, FL, 1993, pp. 119–137.

²⁰Wilson, G. J., and Sussman, M. A., "Computation of Unsteady Shock-Induced Combustion Using Logarithmic Species Conservation Equations," *AIAA Journal*, Vol. 31, No. 2, 1993, pp. 294–301.

²¹Kruczynski, D. L., and Nusca, M. J., "Experimental and Computational Investigation of Scaling Phenomena in a Large Caliber Ram Accelerator," AIAA Paper 92-3245, July 1992.

²²Sinha, N., York, B. J., Dash, S. M., Drabczuk, R., and Rolader, G. E., "Progress Towards the Development of Transient Ram Accelerator Simulation as Part of the U.S. Air Force Armament Directorate Research Program," AIAA Paper 92-3248, July 1992.

²³Ahuja, J. K., and Tiwari, S. N., "A Parametric Study of Shock-Induced Combustion in a Hydrogen-Air System," AIAA Paper 94-0674, Jan. 1994.

²⁴Li, C., Kailasanath, K., and Oran, E. S., "Detonation Structures Behind Oblique Shocks," *Physics of Fluids*, Vol. 6, No. 4, 1994, pp. 1600–1611.

²⁵Grismer, M. J., "Numerical Simulations of Steady and Unsteady Oblique Detonation Phenomena with Application to Propulsion," Ph.D. Dissertation, Univ. of Notre Dame, Notre Dame, IN, 1994.

²⁶Chakravarthy, S. R., and Osher, S., "Computing with High-Resolution Upwind Schemes for Hyperbolic Equations," *Lectures in Applied Mathematics*, Vol. 22, 1985, pp. 57–86.

²⁷Dadone, A., and Grossman, B., "Characteristic-Based, Rotated Upwind Scheme for the Euler Equations," *AIAA Journal*, Vol. 30, No. 9, 1992, pp. 2219–2226.

²⁸Thompson, K. W., "Time Dependent Boundary Conditions for Hyperbolic Systems," *Journal of Computational Physics*, Vol. 68, No. 1, 1987, pp. 1–24.

²⁹Hirsch, C., *Numerical Computation of Internal and External Flows, Volume 2: Computational Methods for Inviscid and Viscous Flows*, Wiley, New York, 1990.

³⁰Fickett, W., and Davis, W. C., *Detonation*, Univ. of California Press, Berkeley, CA, 1979.

³¹Lee, H. I., and Stewart, D. S., "Calculation of Linear Detonation Instability: One-Dimensional Instability of Plane Detonation," *Journal of Fluid Mechanics*, Vol. 216, 1990, pp. 103–132.

³²Fickett, W., and Wood, W. W., "Flow Calculations for Pulsating One-Dimensional Detonations," *Physics of Fluids*, Vol. 9, No. 5, 1966, pp. 903–916.

³³Bourlioux, A., Majda, A. J., and Roytburd, V., "Theoretical and Numerical Structure for Unstable One-Dimensional Detonations," *Journal of Applied Mathematics*, Vol. 51, No. 2, 1991, pp. 303–343.

³⁴Chernyi, G. G., "Supersonic Flow Past Bodies with Formation of Detonation and Combustion Fronts," *Problems of Hydrodynamics and Continuum Mechanics*, Society for Industrial and Applied Mathematics, Philadelphia, PA, 1969, pp. 145–169 (English edition).